8

Elastic Waves on Large Concrete Surfaces for Assessment of Deterioration and Repair Efficiency

D. G. Aggelis[1], H. K. Chai[2] and T. Shiotani[3]
[1]*Materials Science & Engineering Department, University of Ioannina,*
[2]*Department of Civil Engineering, Faculty of Engineering, University of Malaya*
[3]*Graduate School of Engineering, Kyoto University*
[1]*Greece*
[2]*Malaysia*
[3]*Japan*

1. Introduction

Most of society's infrastructure supporting certain sectors of human activity is based on cementitious materials. Bridges, highways, water intake facilities and other structures are made of concrete. These structures sustain external function loads, own weight, as well as deterioration by temperature cycles and attack of environmental agents during their useful life span. The number of civil infrastructures built more than 50 years ago may be estimated to several hundreds of thousands worldwide (Chai et al. 2010). The operational efficiency of these structures is of primary importance for economic reasons but mostly for human safety. Concrete structures have ceased to be considered maintenance-free. They should be inspected in regular intervals, their damage level should be evaluated and when necessary, repair action should be applied. Maintenance or repair projects should be based on prioritization as to the importance of the structure and its damage status. Therefore, economic, fast and reliable characterization schemes are highly demanded. In most of the currently available methods of assessment, elastic modulus of material and strength characteristics are the primary criteria of consideration. In order for the information to be obtained, it often becomes necessary that mechanical tests are conducted on samples acquired from the target structure, through extraction of cores or other similar exercises, which turn out to be inflicting further damage to the already-degraded target structure. In addition, considering the nature of these exercises, which are usually adopted at selected locations, the assessment results are local and often not representative for the overall structure. Recently, extensive research has been reported in elastic wave-related techniques resulting in reliable assessment of the structural condition of actual concrete materials and structures. The characterization of concrete structures by Non Destructive Testing (NDT) and specifically stress wave methods produces mainly qualitative but very important results concerning damage. The surface layer of concrete suffers the most of environmental degradation as well as maximum stresses particularly by flexural loading. It is reasonable

therefore, that considerable deterioration initiates from the surface. The deterioration is often observed in the form of small-scale cracking or macroscopic surface breaking cracks which can propagate to the interior and accelerate the deterioration of the whole structure, especially if the embedded metal reinforcement is exposed to various environmental agents. According to the results, proper repair action can be taken and therefore, the functionality of a structure can be extended. This is extremely important bearing in mind that the cost of building new infrastructure is much higher compared to a focused repair project aiming at extending the service life of the structure for decades.

The most widely used feature in elastic wave NDT is pulse velocity, which is correlated with the damage degree. Despite its rough results, pulse velocity monitoring of large concrete structures is of great significance since it offers a general estimation of the condition and enables proper repair action. Empirical correlations between pulse velocity and damage or strength have been exploited for a long time (Jones 1953, Kaplan 1959, Anderson and Seals 1981, Popovics 2001). It is accepted that pulse velocity, even though not extremely sensitive to damage (reduced prior to final failure by a percentage of not more than 20%), is very indicative of the internal conditions of the material (Van Hauwaert et al. 1998, Shiotani and Aggelis 2009). It possesses essential characteristics making it the most widely accepted and used parameter in concrete NDT. One of these advantages is its direct relation to the elastic constants through well known elasticity relations (Sansalone & Streett 1997, Naik et al. 2004). This way, elastic waves measurements enable the estimation of the modulus of elasticity and consequently projection to the strength of the material through empirical relations (Kaplan 1960, Keating et al. 1989, Shah et al. 2000 , Monteiro et al. 1993, Philippidis & Aggelis 2003).

Another essential feature of pulse velocity is its independence to the propagation distance. Pulse velocity is firmly fixed to the elastic constants and nominally its value does not exhibit changes with distance like other parameters, e.g. amplitude and frequency which are continuously decaying due to attenuation (Landis and Shah 1995, Owino and Jacobs 1999, Jacobs & Owino 2000). In addition to the well known use and interpretation of pulse velocity, frequency and dispersion features have recently been studied with the aim of more accurate characterization concerning the damage content and characteristic size (Aggelis & Philippidis 2004, Philippidis & Aggelis 2005, Punurai et al 2006, Aggelis & Shiotani 2007a, In et al. 2009, Chaix et al. 2006). Dispersion originates from inhomogeneity and hence the velocity dependence on frequency should be much more evident in damaged than in healthy media. Concrete is inhomogeneous by nature due to porosity and aggregates and exhibits moderate dispersive trends (Philippidis & Aggelis 2005, Punurai et al. 2006). Nevertheless, cracks due to size and severe impedance mis-match with the matrix material, are stronger scatterers of elastic waves and influence wave propagation more effectively than the inherent inhomogeneity of the material.

As aforementioned, concrete structures suffer deterioration in the form of distributed micro-cracking as well as macroscopic surface breaking cracks. Cracking allows water and other chemical agents to penetrate into the material, further deteriorating the structure, oxidizing the reinforcement and finally compromising its load bearing capacity (Ohtsu & Tomoda 2008). It is desirable to mitigate these deteriorating actions or even strengthen the structure by repair. Repair can take place in the form of cement injection either targeted to seal

specific macroscopic cracks (Aggelis & Shiotani 2007b, Thanoon et al. 2005, Issa & Debs 2007, Yokota & Takeuchi 2004), as well as a measure to reinforce the whole surface applying injection in a pattern of boreholes on the surface of the structure (Shiotani et al. 2009, Shiotani & Aggelis 2007). Concerning specific macro-cracks, their depth can be evaluated by ultrasound either by the travel time of the longitudinal wave refracted from the tip of the crack, or the amplitude of the surface Rayleigh wave that survives beneath the crack (Doyle & Scala 1978, Hevin et al. 1998, Liu et al. 2001, Pecorari 2001, Song et al. 2003, Zerwer et al. 2005, Aggelis et al. 2009). The same measurements can be repeated after application of grouting agent in order to estimate the efficiency of repair. However, although this can be done for specific surface breaking cracks it would be not be practical for a large concrete surface that normally has numerous cracks. Therefore, although specific cracks may be indicatively targeted for detailed measurements, it is also desirable to establish a way to evaluate the general conditions of a large area of the structure both before and after repair. The relative change of wave parameter values before and after maintenance actions offers a deterministic measure of repair efficiency (Kase & Ross 2003, Aggelis & Shiotani 2007b, Shiotani et al. 2009, Aggelis et al. 2009) which otherwise should be based solely on empirical criteria. This way the effectiveness of the repair can be quantified by the change of wave features, as elastic waves propagate in long distances through the material and gather information from different parts. In the present chapter, distributed micro-cracking on large concrete surfaces is examined by elastic waves before and after repair. Results are presented from an actual old and deteriorated structure, as well as a large concrete block with simulated defects inside. It is exhibited that complementary use of Rayleigh and longitudinal waves is appropriate for the evaluation of initial condition and repair efficiency, while combined use of wave velocity and major frequency, as well as their dependence (dispersion) enhances the evaluation of repair. This kind of dispersion effects are attributed to inhomogeneity (Tsinopoulos et al. 2000) and are diminished after repair. Additionally, development in computer and electronic engineering enables tomography reconstruction of the interior characterized by the value of the propagation velocity of either longitudinal or Rayleigh waves, which can be related directly to the mechanical properties of the material (Sassa 1988, Kepler et al. 2000, Kobayashi et al. 2007, Shiotani et al. 2009, Aggelis et al. 2011). For the full field measurement of a large concrete surface, the newly developed Rayleigh wave tomography methodology is discussed showing the potential to successfully map the subsurface defects, exploiting the connection between penetration depth and applied wavelength (Chai et al. 2010). The chapter comprehensively reviews the current practice in structural health monitoring of real structures using elastic waves, in addition to discussing new trends and features for more detailed assessment of the damage condition.

2. Longitudinal and Rayleigh waves

Wave propagation is strongly affected by the elastic properties and density of constituent materials. Longitudinal wave velocity is given in Eq. (1):

$$C_P = \sqrt{\frac{E}{\rho}\frac{\left(1-v\right)}{\left(1+v\right)\left(1-2v\right)}} \tag{1}$$

where E is the elasticity modulus, ρ is density, and v is the Poisson's ratio.

It has been correlated with strength (Kaplan 1959, Kaplan 1960, Kheder 1999, Qasrawi 2000, Naik et al. 2004) and damage (Van Hauwaert et al. 1998, Ono 1998, Mikulic et al. 1999, Aggelis & Shiotani 2008a, Shiotani & Aggelis 2009) of concrete materials, offering rough but valuable estimations because the damage condition influences the mechanical properties and, hence, the wave speed. Employing a number of sensors, the velocity structure of the material can be constructed and the internal condition can be visualized, highlighting the existence of voids or cracks (Sassa 1988, Kepler et al. 2000, Kobayashi et 2007, Aggelis & Shiotani 2007b, Shiotani et al. 2009). Furthermore, the use of Rayleigh (or surface) waves seems quite suitable for surface opening cracks investigation, since they propagate along the surface of the structure. Additionally, they occupy higher percentage of energy than the other types of waves. For example, as mentioned in (Graff 1975) a point source in a homogeneous half space radiates 67% of its energy in the form of Rayleigh waves, while only 7% in compressional ones. Moreover, since they are essentially two-dimensional, their energy does not disperse as rapidly as the energy associated with three-dimensional dilatational and shear waves. Specifically, their amplitude is inversely proportional to the square root of propagation distance while for a longitudinal wave the amplitude is inversely proportional to the distance (Owino & Jacobs 1999). This makes them more easily detectable than other kinds of waves, as will also be discussed in the present text. The distinct difference from longitudinal waves concerns the particle motion which is elliptical with the vertical component greater than the horizontal, as opposed to the unidirectional oscillation of the particles in longitudinal waves (Graff 1975). The Rayleigh motion decreases exponentially in amplitude away from the surface (Jian et al. 2006). Practically, the penetration depth of these waves is considered to be similar to their wavelength (Sansalone and Streett 1997, Jian et al. 2006). The velocity of surface Rayleigh waves, C_R, which will be also discussed in this chapter, is given by (2):

$$C_R = \frac{(0.87 + 1.12v)}{1+v} \sqrt{\frac{E}{2\rho(1+v)}} \tag{2}$$

From equations (1) and (2) it is derived that by measuring both longitudinal and Rayleigh velocities, apart from the Young's modulus, the Poisson's ratio can be calculated as well.

3. Experimental part

3.1 Repair

On the surface of the old concrete structure (dam) numerous cracks were observed, as is typical due to long exposure to freezing-thawing cycles, and water attack. Repair was applied by cement injection in three different ways. First, cement injection was conducted from the opening of the thicker cracks using syringes, see Fig. 1. As to thin cracks, they were repaired by surface application of cement. Finally, cement was injected in a pattern of boreholes on the surface using a constant pressure, as described in (Shiotani & Aggelis 2007). The actual result is that empty pockets in the structure created by cracks or extensive porosity were filled with cementitious material. This material is initially liquid in order to penetrate to the thin crack openings, but due its cementitious nature, hydration reaction transforms it into a stiff inclusion, sealing the crack sides. It results in considerable decrease of permeability which is crucial for water intake facilities and restores some of the load

bearing capacity since voids are replaced by a stiff material reinforcing the structures cross section. Concerning initial crack depth evaluation, some of the cracks can be interrogated by longitudinal or Rayleigh waves (Doyle et al. 1978, Liu et al. 2001, Tsutsumi et al. 2005, Aggelis et al. 2009). However, given the large number of cracks this is not practical. A measure of the quality of the entire surface must be obtained in a time-effective manner.

Fig. 1. (a) Multiple locations of injection on the surface, (b) detail of the injection point.

3.2 Wave measurements

In order to estimate the condition of the material elastic wave measurements were applied before and after repair. In the specific case, three vertical arrays of four sensors were attached using a rectangular pattern to record the surface response, as seen in Fig. 2. All three dimensions of the concrete block (dam pier) were much larger than the monitored area and the wavelength, and therefore, no influence was expected to either longitudinal or Rayleigh waves. Excitation was conducted by a steel ball (35 mm in diameter) resulting in a frequency peak of approximately 10 kHz (see Fig. 3(a)) and a longitudinal wavelength of approximately 400 mm while the Rayleigh wavelength is of the order of 200 mm. The excitation was consecutively conducted near each sensor (which acted as a trigger) and the rest acted as receivers. Therefore, several paths (all possible combinations between two individual sensors) with different lengths were examined. The horizontal spacing was 1.2 m, the vertical 1.5 m, while the longest paths corresponding to the largest diagonals of the whole monitored area were 5.1 m long. The sensors were acoustic emission transducers, namely Physical Acoustics, PAC, R6 sensitive at frequencies below 100 kHz. The acquisition system was a 16 channel PAC, Mistras operated on a sampling frequency of 1 MHz. The sampling time of 1 μs, resulted in an error lower than 0.3%, since even for the shortest distances of 1.2 m, the transit time was approximately 300 μs. The sensors were attached on the surface using electron wax.

Pulse velocity was measured by the time delay of the first detectable disturbance of the waveform. As to the Rayleigh velocity, the reference point used for the measurement was the first peak of the Rayleigh burst that stands much higher than the initial, weaker longitudinal arrivals (Sansalone & Streett 1997, Qixian & Bungey 1996, Aggelis & Shiotani 2007a, 2008b) (see Fig. 3(b)).

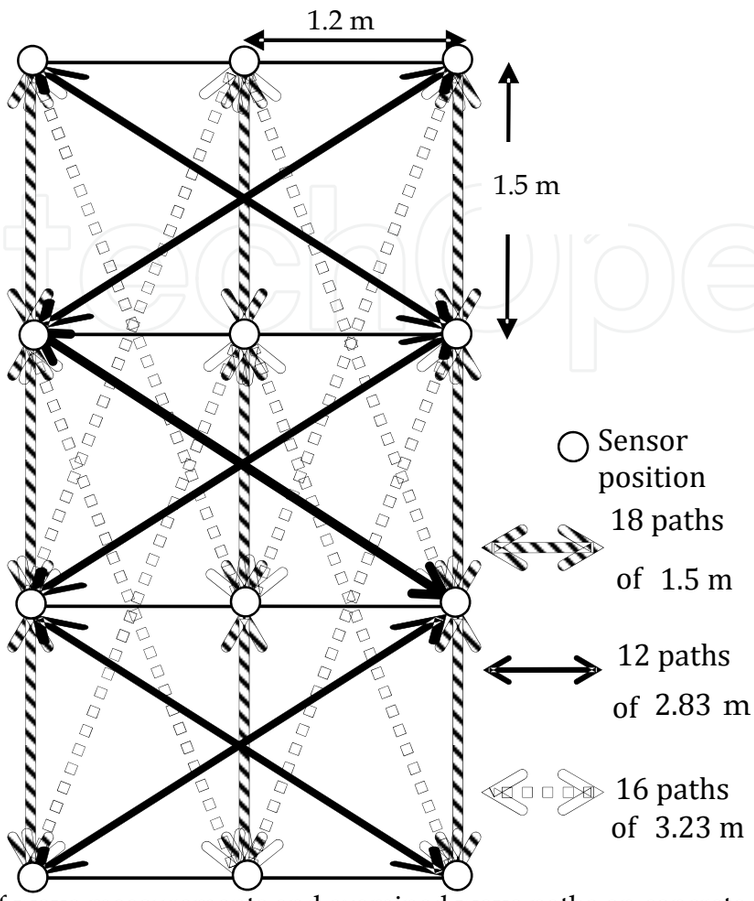

Fig. 2. Pattern of wave measurements and examined wave paths on concrete surface.

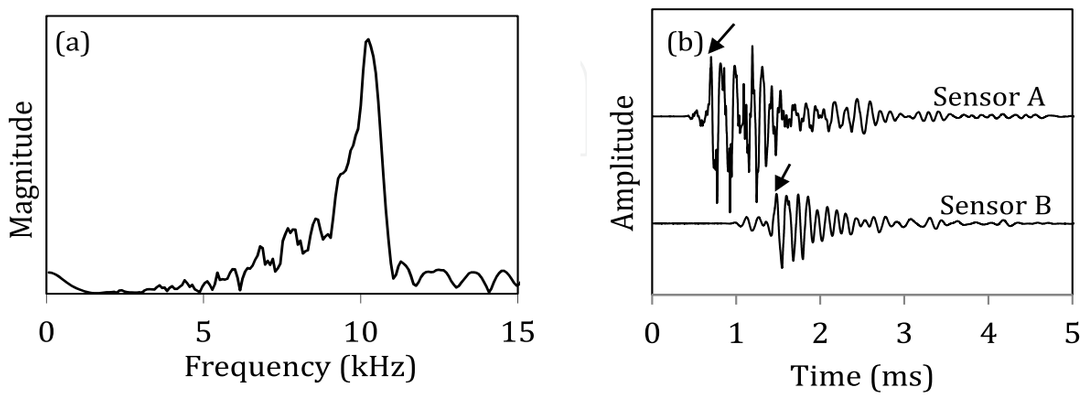

Fig. 3. (a) Frequency spectrum of the excitation, (b) Typical waveforms for sensors at different distances from the excitation.

4. Results

4.1 Wave velocity

Figure 4 depicts the longitudinal velocity as a function of the propagation distance. It is clear that a strong dependence on the distance exists. As already mentioned, nominally wave velocity depends on the elastic constant and not on the travel path. However, there are several reasons that impose this phenomenon. One is the typical crack density compared to the length of the wave path. The possibilities that a short path is crack-free, are higher than a longer one. Therefore it is reasonable that the highest velocities are exhibited at short quarters. Additionally, attenuation effects are accumulated reducing the signal amplitude for longer propagation. This hinders the correct identification of the waveform's leading edge for signals collected at large distances and thus the velocity is underestimated. This can be considered as an indirect effect of damage on the velocity, through the difficulty on interpretation that the attenuation imposes.

The average velocity measured for the short paths of 1.2 m before repair averages at 4500 m/s, while for the longest paths of 5.1 m it is below 4000 m/s. After repair and allowing for a period of two weeks for the injection cement to hydrate properly, the curve is elevated by about 250 m/s, as seen in Fig. 4. This corresponds to an increase of more than 5%, from 4228 m/s to 4455 m/s.

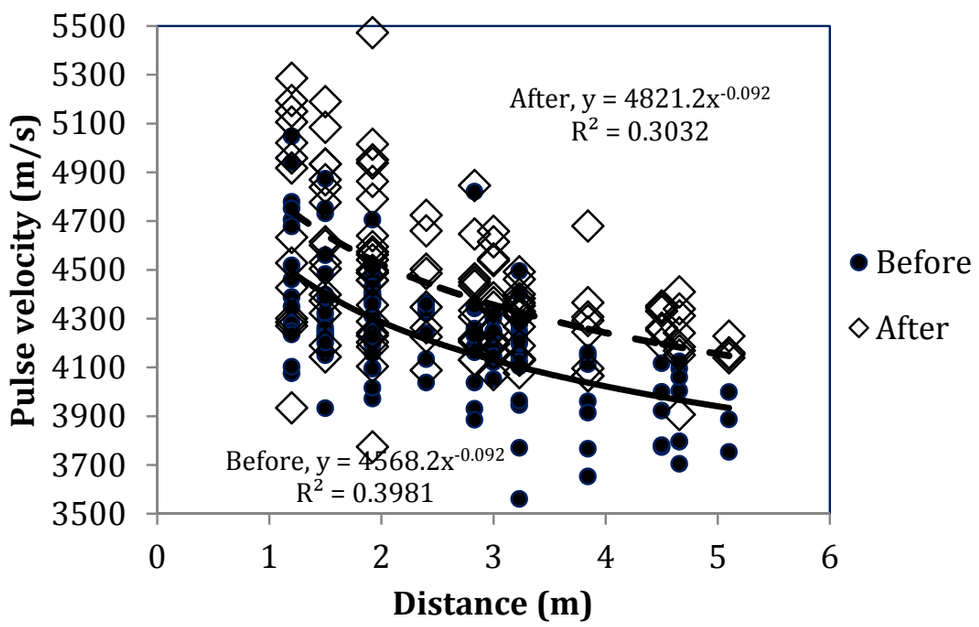

Fig. 4. Pulse velocity vs. propagation distance for different stages of repair.

As to Rayleigh waves, the dependence on the distance is much weaker both before and after repair, as seen in Fig. 5. The reason is connected to the Rayleigh wave measurement, since it uses a strong reference peak (see Fig. 3(b)), much higher than the noise level. The Rayleigh velocity averages at 2235 m/s before and 2363 m/s after repair, being increased by more than 5%, similarly to the longitudinal velocity.

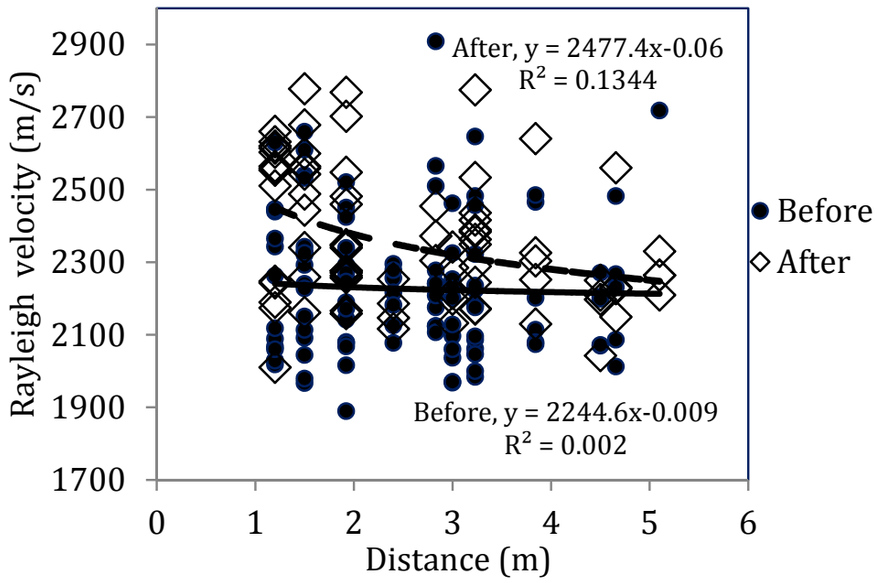

Fig. 5. Rayleigh velocity vs. propagation distance for different stages of repair.

It is mentioned that the average increase is the result of the velocity change for the individual travel paths which can differ considerably from point to point. Fig. 6 shows the velocity change for all individual measurement positions. The large majority of points showed an increase, while a smaller population exhibited decrease. Therefore, while the overall increase is considered satisfactory, examination of the change point by point enables further investigation of specific points that exhibited velocity decrease unexpectedly.

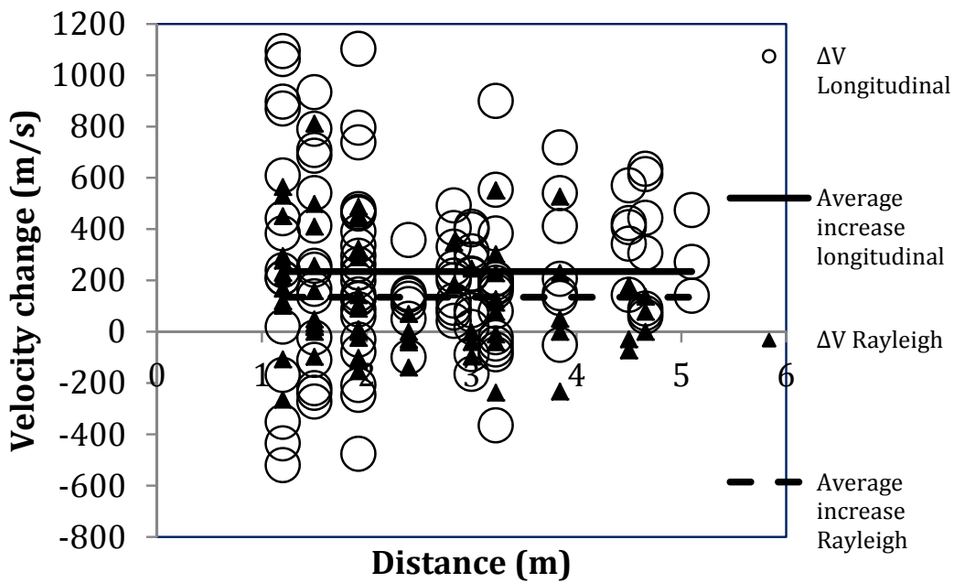

Fig. 6. Difference of velocity between before and after repair for all measurement points.

The average increase of longitudinal and Rayleigh velocities can be translated to elastic modulus improvement by Eqs. (1) and (2). Before repair the effective elastic modulus is calculated at the value of 34.5 GPa, while after repair it is calculated at 37.9 GPa, corresponding to an improvement of approximately 10%. This shows the efficiency of the repair action. It is possible that after full hydration of the injected cement, this increase would be even higher. However, one point needs attention. This is the environmental temperature that influences the hydration rate. In cold environments hydration is delayed and thus the material is gaining rigidity with a slow rate. It has been seen that elastic wave measurements immediately after injection and before the injection material hardens can show the opposite of the desired result (Aggelis & Shiotani 2009, Shiotani et al. 2009). This is due to scattering on the soft pockets of grout which lowers the velocity for a limited time period. Although this phenomenon is normal, and has been recently explained, it contradicts the common knowledge that velocity should always rise after repair. Therefore, it could be misleading and therefore, it is suggested that measurements for repair evaluation are conducted after a sufficient period of time for the cementitious repair agent to cure.

4.2 Pulse frequency

As mentioned in the experimental part, the impact excited a waveform with major frequency components below 20 kHz. As any pulse propagates through inhomogeneous and possibly damaged concrete, the higher of its frequency components are influenced more severely. This change of spectrum can be well monitored by the "central frequency", C (Aggelis & Philippidis 2004, Shiotani and Aggelis 2009). In the specific case the central frequency is calculated as the centroid of the FFT of the waveforms up to 40 kHz:

$$C = \frac{\int_0^{40} fM(f)df}{\int_0^{40} M(f)df} \tag{2}$$

where f is the frequency, and $M(f)$ the magnitude of the FFT.

In Fig. 7, the dependence of central frequency on the distance is depicted. Despite the experimental scatter of the points which is expected due to the inhomogeneity of the material, a certain decreasing trend is exhibited both before and after repair. This demonstrates the cumulative effect of the inhomogeneity of the travel path on the frequency content.The average frequency before repair is 12.5 kHz for short propagation distance while it is reduced to 6.8 kHz for the longest paths of 5.1 m. The trend can be fitted quite well with a decaying exponential curve, and is attributed to the stronger attenuation of higher frequencies (Tsinopoulos et al. 2000, Shiotani & Aggelis 2009). Measurements on the same points after repair showed a frequency increase of approximately 2 kHz for any distance, as seen again in Fig. 7. This can be attributed to the filling of the cracks which reduces the material scattering attenuation. It should be mentioned that the frequency is not directly correlated with concrete strength or structural integrity. However, in any case, strength can be estimated only through empirical relations even for pulse velocity. The

importance lies on the comparison between the two stages (before and after repair). Since a frequency upgrade was evident this shows that there was a certain improvement on the structure's surface layer due to void elimination.

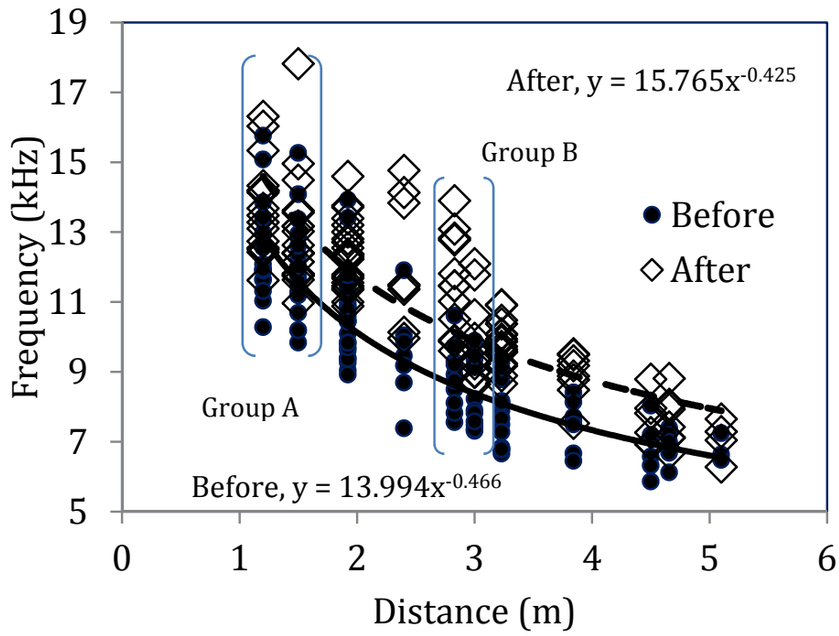

Fig. 7. Central pulse frequency vs. propagation distance for different stages of repair.

4.3 Reliability aspects

At this point it is worth to mention the importance of reliability of the signal acquisition. Strong attenuation due to inhomogeneity and spreading due to long distances decrease the signal level very effectively. This is crucial especially for the pulse velocity measurement, which is conducted by the first detectable disturbance of the received waveform. In case the signal is weak, the first cycle may be of the same level or even lower than the noise level and therefore, the velocity is underestimated. This is a phenomenon that is not widely considered in practical applications. The strength of the signal compared to the noise is measured by the "signal to noise ratio", S/N, which is simply the ratio of the waveforms peak amplitude divided by the average noise level of each waveform. The noise level is calculated by the amplitude of the "pre-trigger"period, the period after each sensor starts acquisition and before the actual wave arrives at the sensor point. In order to see the effect of noise on the measurement of wave parameters, the dependence of pulse velocity, Rayleigh velocity and central frequency are plotted vs. S/N in Fig. 8(a), (b) and (c) respectively. Concerning Fig. 8(a) before repair, an increasing trend of velocity can be found with increase of S/N. It is obvious that for S/N lower than 1000, velocities average around 4000 m/s, while for higher S/N the velocities reach 4500 m/s in average. After repair, as already discussed, the "cloud" of points is elevated to higher velocity (due to elastic modulus restoration) and higher S/N values due to the decrease of scattering attenuation. At the same time, the correlation between velocity and S/N is sufficiently weakened (from

R^2 of 0.26 to 0.07). It can be concluded that when S/N is low (e.g. less than 1000) the velocities are certainly underestimated, while the measurement becomes almost independent for S/N ratios higher than 3000. This is an aspect that should always be considered in field measurements, especially for long distance measurements.

As aforementioned the Rayleigh velocity is calculated by possibly the strongest peak of the waveform (the first peak of the Rayleigh burst) and therefore, it does not crucially depend on the S/N ratio. This is shown in Fig. 8b where the correlation coefficient between velocity and S/N is close to zero. Similar results with pulse velocity with even higher correlation coefficients can be seen in Fig. 8c for the central frequency of the pulse. Before repair there is a very clear increasing trend exhibiting also a quite high correlation coefficient R^2 of 0.61. This shows that when the signal is strongly attenuated and its strength decreases with respect to noise, the higher frequencies are the first to be influenced. The increasing trend holds for the measurements after repair, though in this case the correlation is much weaker.

The discussion of S/N is concluded with its dependence on distance. In any case it is normal that the S/N ratio decreases with distance in any material, since the effect of attenuation is accumulated for longer travel paths. However, it is remarkable to see that the S/N undergoes a change from approximately 6000 for short wave paths (1.2 m) to less than 500 for longer (5.1 m) as depicted in Fig. 9. This change of more than 12 times indicates that the data should be divided in smaller groups in order to exclude the effect of attenuation, when discussing elasticity modulus or dispersion effects, as will be analyzed in the next section. Additionally, after repair, it is evident that the S/N increased and the correlation to distance was certainly reduced from 0.59 to 0.25. It is also characteristic that for the shortest distance (1.2 m) the S/N is quite similar for both conditions (before and after repair) with values 5900 and 6600 respectively. Larger differences are observed for longer paths (>4 m) where the effect of attenuation is accumulated, i.e. less than 400 before and 1250 after repair.

4.4 Dispersion relation

Both longitudinal velocity and frequency decrease exponentially with distance; thus they are correlated with each other, as seen in Fig. 10. The clusters consist of 130 points which is the total number of possible paths between the sensors. Due to inhomogeneity and locality effects there is a certain experimental scatter. However, it is clear that both before and after repair there is a positive correlation showing a certain dependence of velocity on frequency. Nevertheless the average velocity and frequency both increase after repair. Apart from the average longitudinal velocity increase of more than 5%, central frequency increases from 9.6 kHz to 11.1 (change of 15.6%). This kind of simultaneous examination of different features can enhance repair characterization since frequency increase seems to be more sensitive to repair than velocity of longitudinal and Rayleigh waves.

It is understood that the correlations in Fig. 10 include the influence of distance since the measurements are taken for any different distance between 1.2 m and 5.1 m. In order to examine the frequency effect on the propagation velocity excluding the influence of attenuation, the information was processed in small groups of data collected over close distances. Two cases will be indicatively discussed. One group (group A of Fig. 7) includes the data collected at the shortest distances of 1.2 m and 1.5 m (totally 34 points), while the other (group B of Fig. 7) includes the approximately double distances of 2.83 m and 3 m

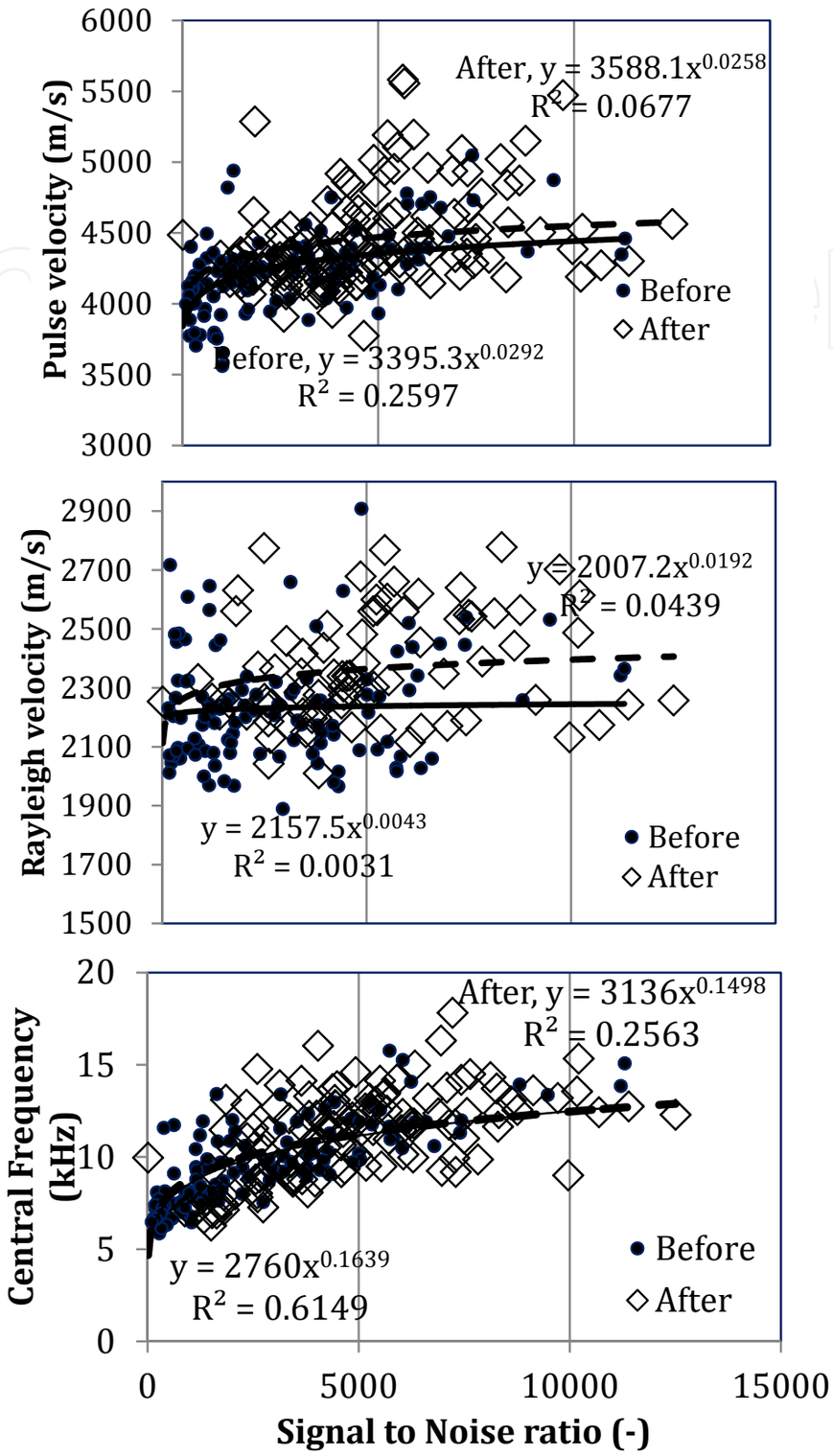

Fig. 8. Wave parameters vs. signal to noise ratio (a) pulse velocity, (b) Rayleigh velocity, (c) central frequency.

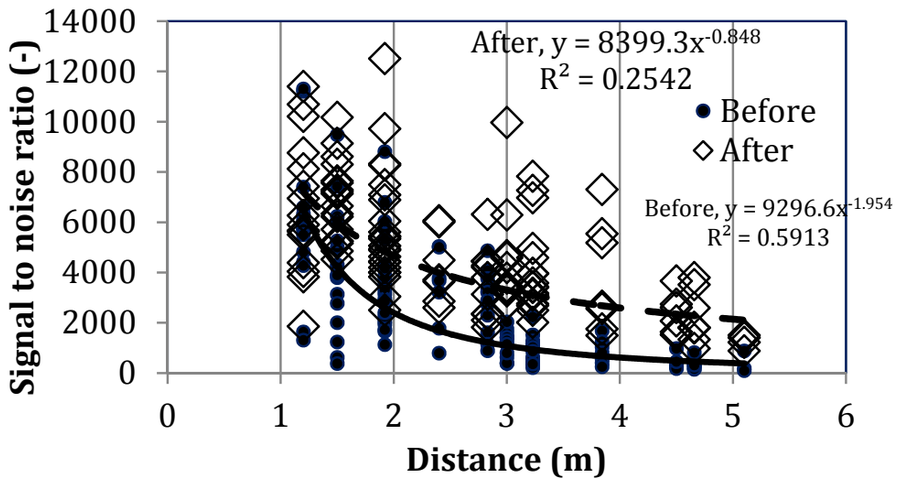

Fig. 9. Signal to noise ratio vs. propagation distance for different repair stages.

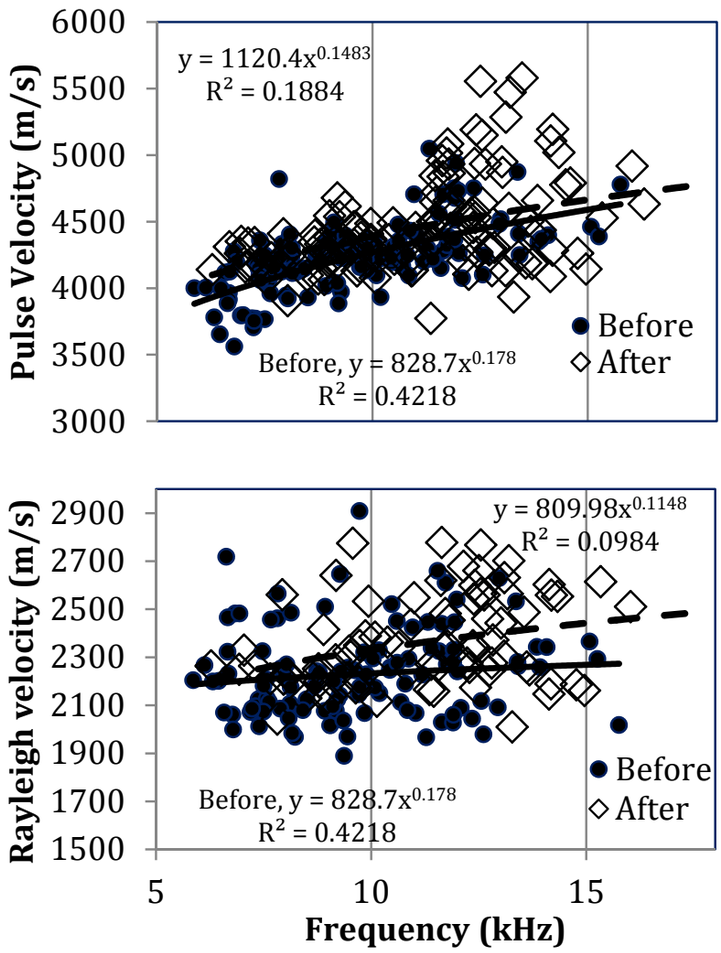

Fig. 10. Pulse (a) and Rayleigh (b) velocity vs. frequency for the total population of measurements.

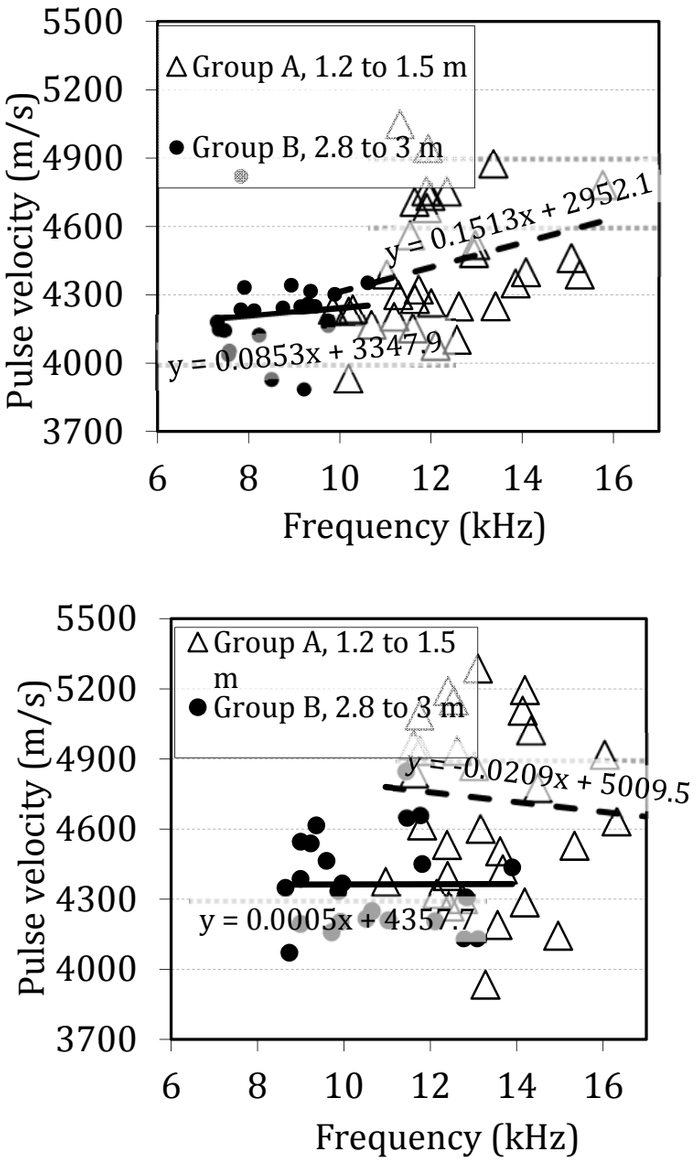

Fig. 11. Pulse velocity vs. Frequency for different length of wave paths (a) before and (b) after repair.

(totally 24 points). For each group, the velocity vs. frequency correlation is depicted in Figs. 11a and b. Since the data in each group are taken from similar distances, the effect of attenuation is eliminated allowing examination of pure dispersion effects within each group. The experimental scatter is high since each travel path in damaged concrete is unique due to the randomness of inhomogeneity. The total population shows a trend that should not be ignored; there is a positive correlation between velocity and frequency before repair. This implies that an increase in frequency content results in a slight increase of pulse velocity. This trend is in agreement with recent dispersion studies on concrete (Chaix et al. 2006, Philippidis & Aggelis 2005, Aggelis and Shiotani 2007, 2008, Aggelis 2009). They reveal that

below 100 kHz the increasing slope of the dispersion curve is steep, while for frequencies around or above 100 kHz the curve reaches a plateau. This dispersion is stronger as the inhomogeneity of the material increases and has been measured for wide frequency bands up to almost 1 MHz (Philippidis & Aggelis 2005, Chaix et al. 2006). In general in all typical particulate composites or porous materials (Kinra & Rousseau 1987, Sayers & Dahlin 1993, Aggelis et al. 2004), phase velocity is lower than the velocity of the matrix for low frequencies, but rises with frequency until reaching approximately the velocity of the matrix. For higher frequencies the velocity does not exhibit serious alterations according to the above mentioned studies.

It is interesting to examine the same correlation after repair. Apart from the general translation of the points to higher velocity and frequency levels for any propagation distance, the slight positive correlation is eliminated for both groups. Cement injection filled cavities and cracks eliminating inhomogeneity to a large extend. Thus, the structure behaved in a less dispersive way. This repair-dependent dispersion should not be ignored as it shows the potential to enhance the rough characterization performed so far in concrete. It is mentioned that all individual distance groups of data exhibited the velocity-frequency dependence. Fig. 11 contains the groups with the largest population. Same behavior concerning the frequency dependence of pulse velocity was observed for through the thickness measurements of elastic waves in concrete pier before and after repair. A certain dispersive trend was exhibited initially, while after the repair material was properly hydrated into the structure, this trend was weakened (Aggelis et al. 2011).

The dependence of Rayleigh velocity on distance and frequency is much weaker than in the case of longitudinal as was seen in Figs. 5 and 10. One possible explanation is the long wavelength compared to the depth of surface-opening cracks. Some surface cracks with wide openings (i.e. 0.2 – 0.4 mm) were targeted using longitudinal and Rayleigh waves for depth measurement (Aggelis et al. 2009). The depth of cracks never exceeded 100 mm while an average value for the depth of the cracks was 35 mm. Rayleigh waves propagating through a depth of more than 200 mm (similar to their wavelength) can "dive" below the shallow defects. Therefore, their dispersion in this case is weaker, since the highest degree of damage is concentrated near the surface, while the propagation of Rayleigh takes place also through deeper, more homogeneous zones. On the other hand, longitudinal waves traveling along the surface are influenced by each surface crack as it poses a discontinuity on their path. This makes their dependence on frequency stronger, as was seen in Figs. 4 and 10. Dispersion should be further studied for material characterization since in a general case, limited dispersion of Rayleigh should imply that defects are shallower than the Rayleigh wavelength offering a means of fast estimation for a large surface.

5. Rayleigh wave tomography

Analysis of elastic wave data certainly offers insight on the structural condition of the material, as was shown above by the changes in wave properties and dispersion. However, one way to further enhance the understanding of the results is visualization. This is one global goal concerning the inspection. Techniques like X-rays, radar, thermography and elastic waves aim to produce ''tomograms" of the structure (Aggelis et al. 2011, Diamanti et al. 2008, Ito et al. 2001, Ohtsu and Alver 2009) in order for the results to be more easily

understood by a general audience (owner of structure or user). For the specific case of near surface damage, the establishment of Rayleigh wave-based tomography technique is beneficial since it materializes single-side assessment, which is particularly useful for certain structures with open access only on one surface, such as tunnels and bridge deck panels. Also using the tomography technique, examination of in-situ structures becomes more realistic because it provides general indications on problematic spots within a relatively short time of execution. These spots could then be assessed by a pin-point approach in a detailed manner to characterize the defect.

5.1 Analytical study of Rayleigh waves propagating in concrete with horizontal crack

To clarify the behaviour of Rayleigh waves impinged by a horizontal crack lying within the concrete sub-surface, a series of wave motion simulations have been conducted. The simulations were conducted using commercial software developed for solving two-dimensional elastic wave propagation based on finite difference method. As illustrated in Fig. 12, the analytical model was generally composed of the concrete medium with four sensors located on the top side of the model at a uniform distance of 100 mm. A point source for generating elastic waves was located 50 mm away from the trigger sensor to the left. The trigger sensor initiate simultaneous recording of waveforms once the incoming of wave was detected. Sensors R1, R2 and R3 were placed to record waveforms at different locations as the generated waves propagate further from the source. In the simulations, the concrete was modeled with the first and second lame constants of 10 GPa and 15 GPa, respectively, and density of 2300 kg/ m^3. Damping of elastic waves in concrete was appropriately defined to simulate waveforms reasonably close to those observed in the experimental measurement. The configuration resulted in a corresponding longitudinal wave velocity of approximately 4200 m/s, a typical value for homogeneous concrete of normal strength. The left, right and bottom sides of the concrete model were configured with infinite boundary conditions in order to avoid reflections and simulate a larger structure geometry. Beside the model of homogeneous concrete, models with an additional 150 x 2 mm void placed parallel to the concrete surface at varying depths from the top side of concrete were also prepared to constitute delamination in concrete.

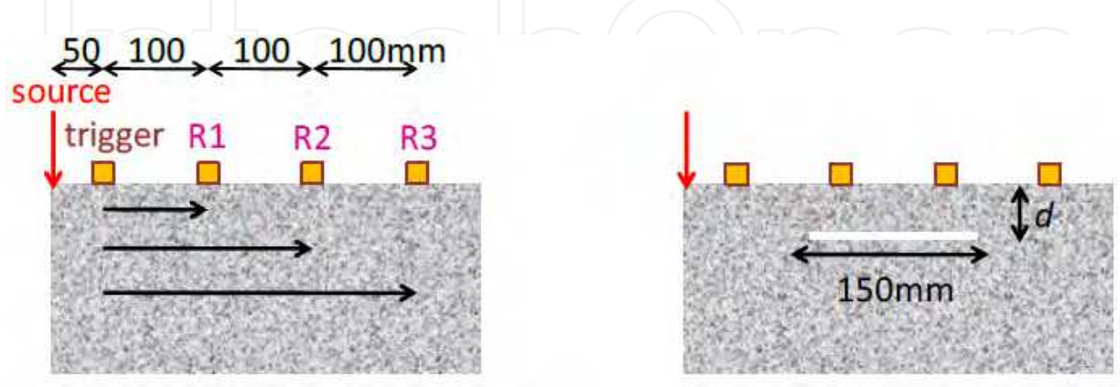

(a) (b)

Fig. 12. Wave motion simulation models, (a) Homogeneous concrete and (b) Inhomogeneity in the form of a horizontal crack

A single-cycle excitation of elastic waves from the point source was generated for all the analytical models. To study the relation between wavelength of Rayleigh waves and depth of delamination that causes distortion, excitations at different frequencies were performed. Hence the simulations produced waveform data for different combinations of excitation frequency and crack depth to serve further analysis purposes.

Fig. 13 presents snapshots of typical simulated cases of elastic waves propagation for the homogeneous model. Knowing that velocity of Rayleigh waves is approximately 57% that of the primary waves for a normal strength concrete (Sansalone and Streett 1997), in the case for 150 kHz excitation (Fig. 13(a)), in which the wavelength was relatively shorter, the separation of Rayleigh wave energy component (with the larger amplitudes) from the primary waves was evident from sensor R1 onwards. The separation became greater as the waves propagated further. For low frequency excitations, namely the 10 kHz one, the separation could not be clearly seen at propagation distance equivalent to that observed for the 150 kHz excitation, because the wavelengths of both wave modes are quite long and therefore overlap at the early distances of propagation before the different propagation velocities separate them (Fig. 13(b)). The separation of Rayleigh waves from longitudinal waves can be justified from the recorded waveforms for the homogeneous concrete model, indicating clearer separation of one full cycle for the 150 kHz excitation when reaching sensor R1. For the waveforms obtained from 10 kHz excitation, even though no complete separation can be observed, Rayleigh waves can be extracted without much difficulty since their arrival was marked by significantly large energy that initiated abrupt increase of amplitude (Qixian & Bungey 1996).

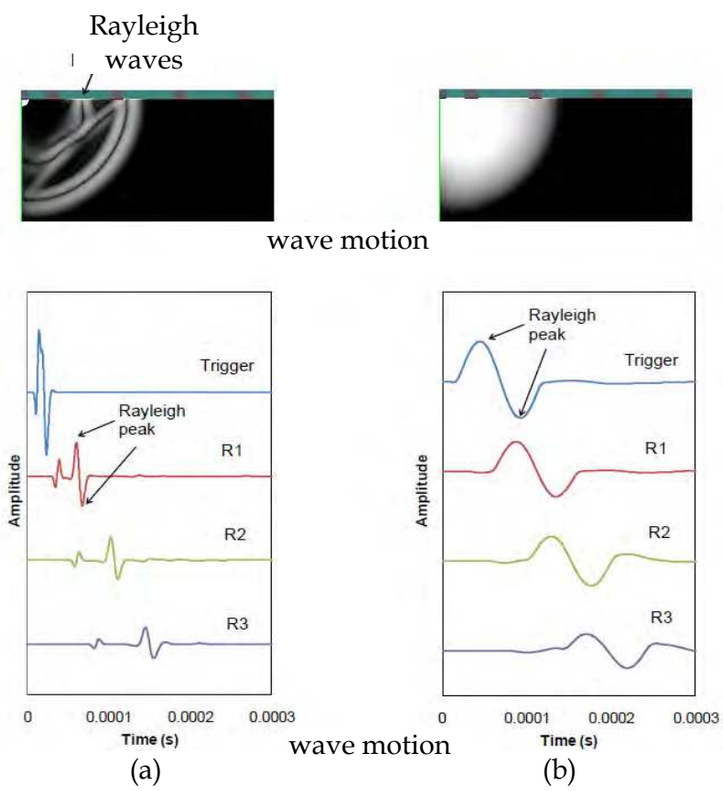

Fig. 13. Snapshots of wave motion and waveform of homogeneous concrete for (a) 150 kHz and (b) 10 kHz excitation frequencies

For the cracked case, when the elastic waves impinged on the crack tip of the delamination, as indicated by snapshots given in Fig. 14, wave diffraction and scattering occur, with some portion of wave energy being "reflected" upwards from the crack-concrete interface to eventually converge with the ones propagating on the surface. Distorted waveforms recorded by sensor R1 indicated a more apparent decrease compared to those from the receivers of the homogeneous concrete model.

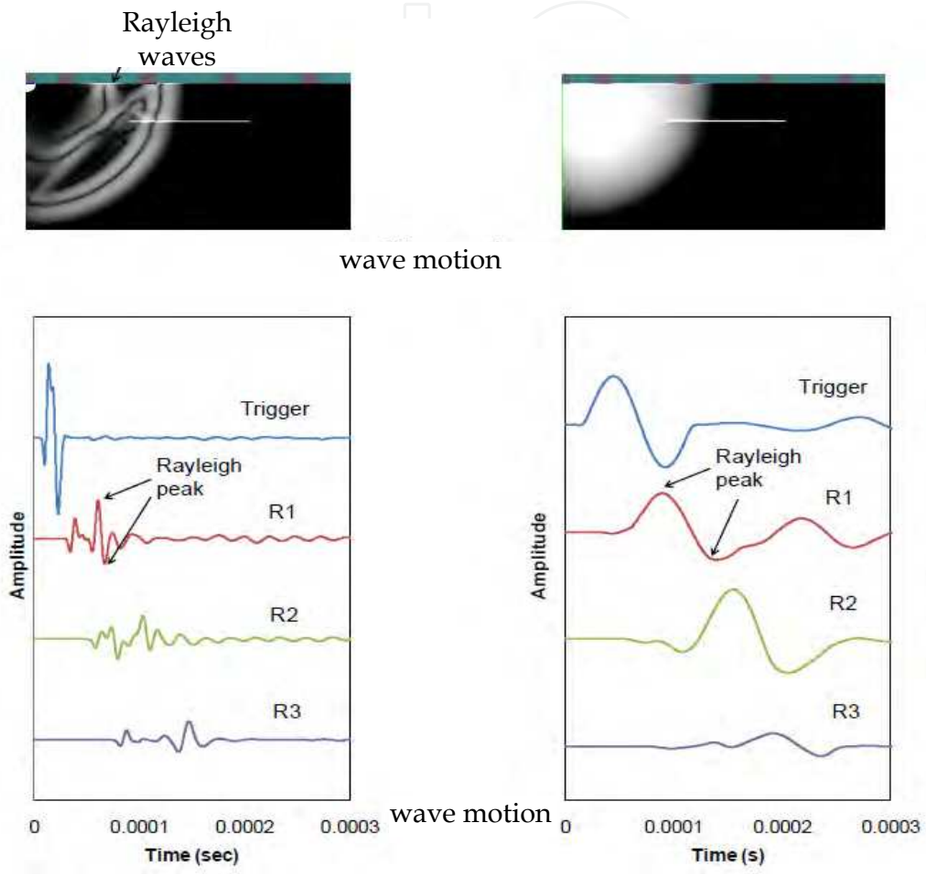

(a) (b)

Fig. 14. Snapshots of wave motion and waveforms of concrete model with a horizontal crack located at 50 mm from top for (a) 150 kHz and (b) 10 kHz excitation frequencies

5.2 Processing for phase velocity

Since the distortion of waves due to the defect could reduce the energy of Rayleigh waves relatively to that of the body waves, which was bound to hamper accurate analysis, the characteristic amplitudes of Rayleigh waves was extracted. The extraction process was carried out simply by "muting" the other wave components so that only the one-cycle Rayleigh waves would remain. The relevant wave components of could be recognized as the maximum amplitudes in both the positive and the negative phases. The processed waveform then yielded a more clear-cut frequency response by the fast Fourier transform (FFT), indicating a characteristic peak frequency belonging to the propagating Rayleigh waves. Observation revealed that the processed waveform for the first sensor have the peak

frequency almost equivalent to the frequency of excitation as configured in the simulation, suggesting that this frequency value could be regarded as the characteristic frequency of the generated Rayleigh waves.

Figure 15 plots the travel time of Rayleigh waves with excitation frequency of 20 kHz against distance of propagation for the homogeneous concrete model. The travel time was obtained by taking the time of positive peak arrival as acquired by the receivers R1, R2 and R3 with reference to the trigger. The gradient of linear regression could be inversed to yield a propagation velocity of 2398 m/s.

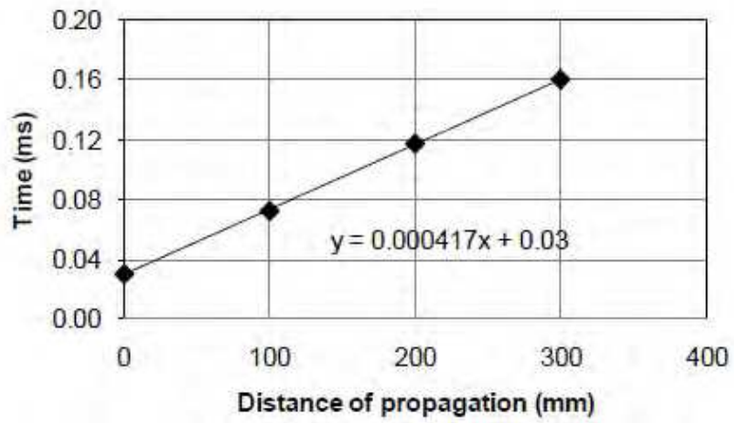

Fig. 15. Linear correlation between arrival time and propagation of Rayleigh waves with 20 kHz excitation frequency

In order to take into account the possible dependence between velocity and frequency which is expected in materials like concrete, especially when they contain inhomogeneity, the "phase velocity" curve can be calculated. The whole procedure is explained in (Sachse & Pao, 1978 and Philippidis & Aggelis, 2005). It includes Fourier transformation of the time domain signals recorded at different positions on the surface of the material. The phase of the signals is unwrapped and phase difference ($\Delta\Phi$) for each frequency is calculated. Then by the knowledge of the separation distance between the receivers, Δx, the velocity for each phase (frequency component) of phase velocity V_{ph} can be derived by the following equation:

$$V_{ph} = \lambda f = \left(\frac{2\pi\Delta x}{\Delta\emptyset}\right) f \tag{3}$$

where λ is the wavelength, f is the frequency for which the phase difference is calculated. By plotting the phase velocity versus the frequency within the bandwidth, i.e. dispersion curve, the change of phase velocity of Rayleigh waves with regards to frequency can be examined. The results can also be used to calculate theoretical wavelength of Rayleigh waves for the respective excitations. Fig. 16 shows exemplary dispersion curves for all the three trigger-receiver combinations in the case for the homogeneous concrete and that with a horizontal crack at 25 mm depth, which were acquired from data with 20 kHz of excitation frequency. The phase velocity for the homogeneous concrete corresponding to 20 kHz was averaged to a value of 2317 m/s, which was very close to that obtained by taking into account the arrival

time of Rayleigh wave peak amplitude. As can be seen from the figures, the dispersion curves were seemingly uniform for the case of homogeneous concrete model, indicating that the phase velocity for each frequency component was quite similar within the bandwidth of excitation. On the other hand, for the models with horizontal crack, the dispersion curves for all the three trigger-receiver combinations exhibited considerable differences and were all translated to lower values. The average phase velocity at the excitation frequency of 20 kHz was calculated as 1723 m/s, which was lower than that obtained for the homogeneous concrete model. Considering that the penetration depth for Rayleigh waves can be equivalent up to its wavelength, it can be inferred that the generated Rayleigh waves in this particular case, which has a calculated wavelength of approximately 110 mm, was effectively distorted by the horizontal crack at 25 mm depth to exhibit translation of phase velocity to lower values as a result of the change in propagation behavior.

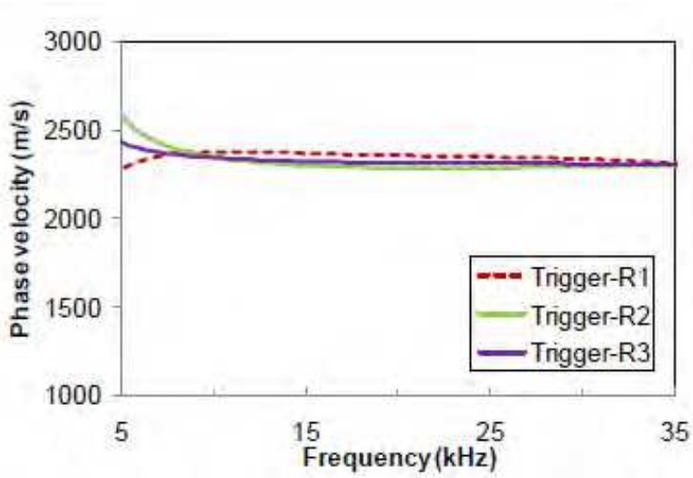

(a)

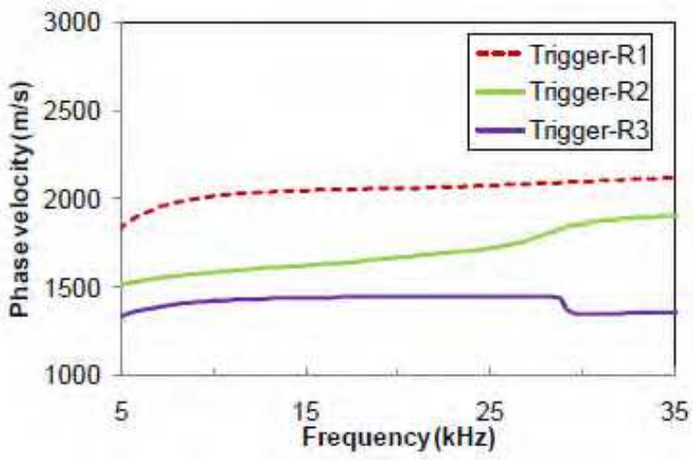

(b)

Fig. 16. Dispersion curve computed for data by excitation frequency of 20 kHz, (a) homogeneous concrete and (b) horizontal crack at 50 mm from top

5.3 Velocity change

The average phase velocity values at respective excitation frequencies were obtained from the models with delamination and normalized with those of the homogeneous concrete model to obtain the "velocity index" for facilitating comparison. The velocity indices were arranged in accordance with the depth of delamination depth, as plotted in the form of bar charts given by Fig. 17. The bars in the charts were classified under two distinct groups: data with the theoretical wavelengths equal or greater than the delamination depth ($d \geq \lambda$); and those of the opposite condition ($d < \lambda$). The data with $d \geq \lambda$ gave lower velocity index compared to the data with $d < \lambda$ in general. Among the simulated cases, the velocity index dropped most noticeably for d = 25 mm, where the soundness indices have decreased to as low as 0.68. In cases where d = 150 mm and 200 mm, although velocity indices of lower than 1.00 were also obtained for $d < \lambda$, the decrease was comparatively small. This could bear the inference that the generated waves have only been slightly disturbed by the horizontal crack although the penetration depth was greater (assuming equivalent to one wavelength) than the crack depth. In other words, the penetration depth was essentially less than the wavelength.

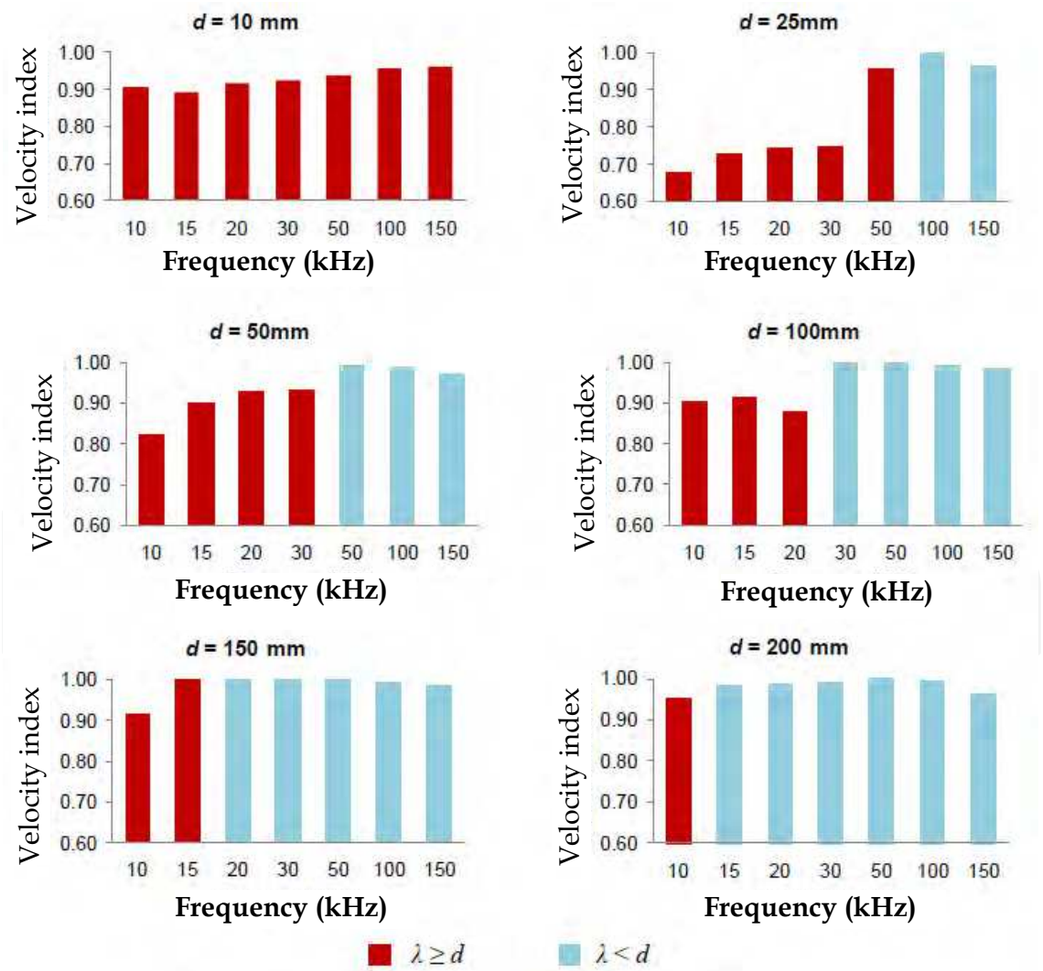

Fig. 17. Velocity indices for different cases of crack depth

Slight decrease in velocity indices in the cases of $d \geq \lambda$ was in general observed in the simulated results. The decrease could be attributed to slight change in the inherent nature of the simulated waves subject to the combinations of crack depths and excitation frequencies. As implied by the findings, inhomogeneity introduced by the presence of horizontal crack in concrete tended to produce variation of phase velocity, even though the decrease would be less significant in some cases. Further examination revealed that the wavelength should be at a minimum of 2.5 times greater than the depth of defect in order to constitute a decrease of at least 10% (velocity index = 0.9) in phase velocity.

5.4 Development of Rayleigh wave tomography

5.4.1 Principle of travel time tomography

A typical travel time tomography involves a unique algorithm that performs iterative computations to reconstruct the velocity profile of a measured object from the picked travel time of elastic waves, which can be obtained in the form of observed data through measurement at selected locations on the object. In ray theory, the travel time, t is computed from the integral of the slowness along a given ray path l

$$t = \int_l \mathrm{d}t = \int_l \frac{1}{v}\mathrm{d}l = \int_L s\mathrm{d}l \tag{4}$$

where v is the velocity, s is the slowness (reciprocal of velocity) and dl is the length element. If a model is subdivided into M cells of constant slowness, s_i for each corresponding segment length l_i, the integral product can be totalled as

$$t = \sum_{i=1}^{M} l_i s_i \tag{5}$$

The above equation can be expressed in a matrix-vector form:

$$\mathbf{t} = \mathbf{L}\mathbf{s} \tag{6}$$

where $\mathbf{t}$ is the travel time vector and $\mathbf{s}$ is the vector of s_i. $\mathbf{L}$ is a matrix describing the ray path segments. The matrix is generally sparse since each ray would cover only a limited number of cells. Equation (6) is solved to simulate a velocity distribution that can explain the measured travel times. Although the ray propagation itself is considered as a linear operator, the inverse problem can become non-linear, which has to be solved using iterative process. With a fundamental model $\mathbf{s}^0$, new models are computed successively based on the discrepancy of data and model response by solving

$$\mathbf{s}_{k+1} = \mathbf{s}^k + \Delta\mathbf{s}^k = \mathbf{s}^k + \mathbf{L}^{\dagger}(\mathbf{s}^{\mathrm{k}})(\mathbf{t} - \mathbf{L}(\mathbf{s}^{\mathrm{k}})\mathbf{s}^{\mathrm{k}}) \tag{7}$$

with $\mathbf{L}$ recomputed and so on, whereby $\mathbf{L}^{\dagger}$ is the used inverse operator.

The computation process is commonly known as the ray tracing procedure, for which the simultaneous iterative reconstruction technique (SIRT) is adopted. The ray paths are usually restricted to the edges of the mesh and a weighted shortest path problem has to be solved. Since not every path can be used, or there is insufficient observed data, the computed travel times are always not accurately estimated in the first few iterations. The accuracy is improved following increasing refinement in the computation to reduce discrepancy.

5.4.2 Experimental measurement of concrete slab

To investigate the feasibility of Rayleigh wave properties as the observed data for tomography reconstruction to visualize defect in concrete, laboratory experiment was carried out to measure and evaluate a concrete slab specimen. The specimen was a 1500 x 1500 x 300 mm concrete slab of normal strength. Defects in the forms of horizontal cracks in concrete at different depths were modelled by including four 5 mm-thick circular Styrofoam plates of 300 mm in diameter. The Styrofoam plates were located at 30 mm, 60 mm, 100 mm and 140 mm from the top of concrete surface, respectively, as depicted in Fig. 18. Shown in the same figure also are the arrangement of 16 accelerometer sensors for sensing and recording of elastic waves. The arrangement formed a total of 240 direct ray paths. During the measurement, elastic waves were generated by manually hitting the concrete surface with a ball hammer that has a spherical head of 15 mm in diameter. A 16-channel waveform acquisition system was used to record waveforms at an interval of 5 μs for a total of 4096 samples. Each set of impact was performed by continuing hitting the specimen surface for 5 seconds, which resulted in approximately 20 impacts or waveforms to be recorded by each sensor. In the preliminary processing of signal, the multiple waveforms recorded by the

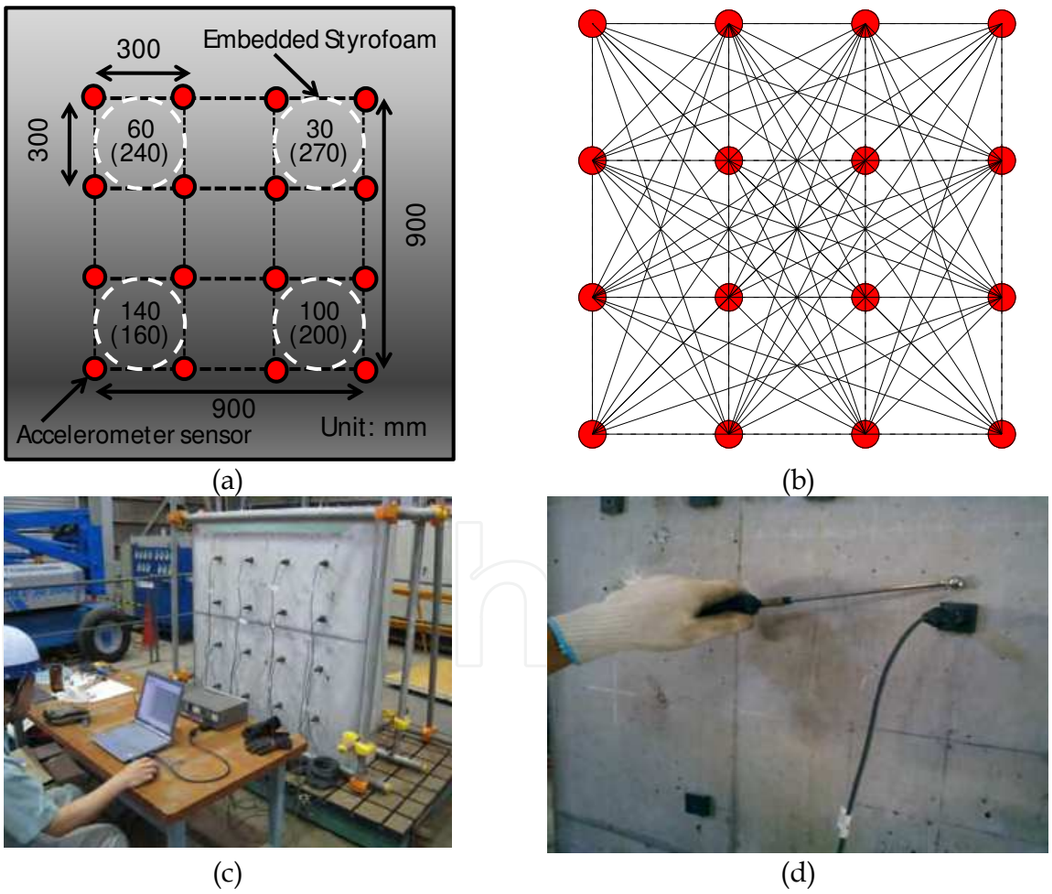

Fig. 18. Tomography measurement on concrete slab: (a) Crack depth and arrangement of accelerometer sensors (() denotes depth from the opposite surface)), (b) Ray path lay-out, (c) Snapshot during measurement, and (d) Generation of elastic waves by hammer with spherical head.

respective sensors would be stacked accordingly to eliminate random noise that could be influential in hampering proper processing in the later stage. Each time the impact was made adjacent to one sensor which has been configured as the trigger, with the others as receivers to detect incoming waves. The acquisition was synchronized in such manner that all 16 channels would start recording at the same time once the trigger channel was excited due to the arrival of elastic waves from the hitting point. The impact and recording process was repeated by subsequently setting the next sensor as the trigger in a pre-determined order until all the sensors have been assigned.

In order to measure the propagation velocity of Rayleigh waves on sound concrete, a separate measurement utilizing nine accelerometer sensors at 150 mm distance was carried out on the sound concrete portion of the same specimen. From the recorded waveforms, the peak amplitudes could be identified because of the large increase in relation to the preceding ones that belonged to the body waves. Taking into account the time of Rayleigh wave arrival, a typical travel time versus distance plot can be drawn as given in Fig. 19. The velocity could be obtained as the inverse of gradient from linear regression, giving an approximate value of 2356 m/s for the sound concrete.

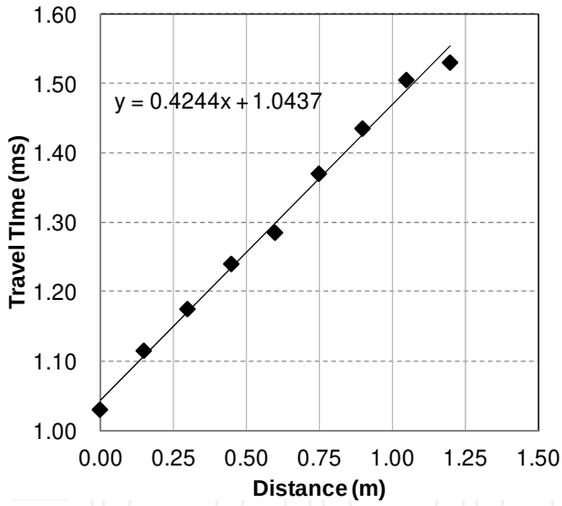

Fig. 19. Time vs. distance plot of Rayleigh waves to estimate propagation velocity

In Fig. 20, an example of time series data and its corresponding FFT frequency spectrum is shown. The frequency spectrum presented two frequency peaks, suggesting the existence of more than one dominant frequency in the waves. By using the similar procedure adopted for the processing of simulation data as discussed earlier, the Rayleigh wave amplitudes was extracted, based on the identification of time window containing the main Rayleigh wave components as anticipated based on the typical propagation velocity. This resulted in a frequency spectrum as given in Fig. 21, clearly indicating only one peak at approximately 9 kHz. Using the measured velocity and peak frequency, the dominant wavelengths was calculated as 240 mm.

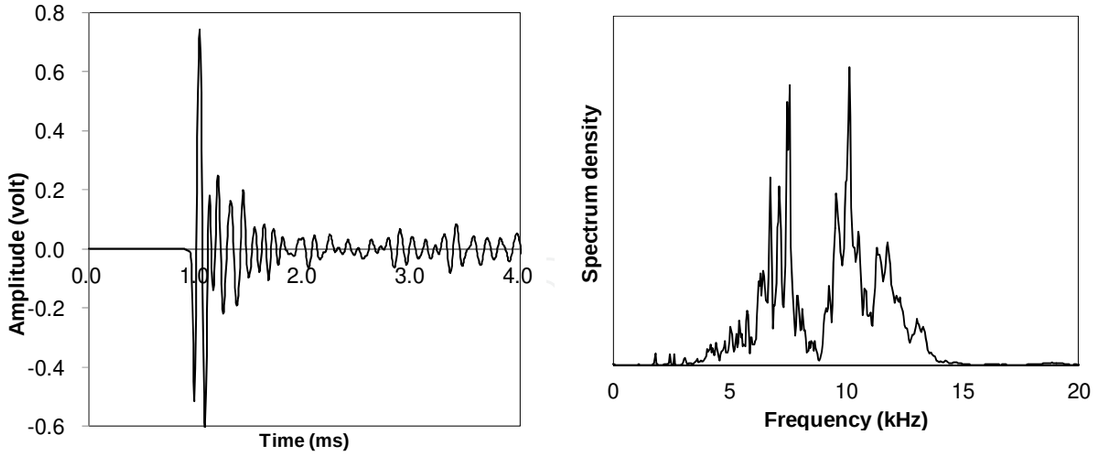

(a) (b)

Fig. 20. Typical measurement results: (a) Time series of original waveforms, (b) Corresponding frequency spectrum

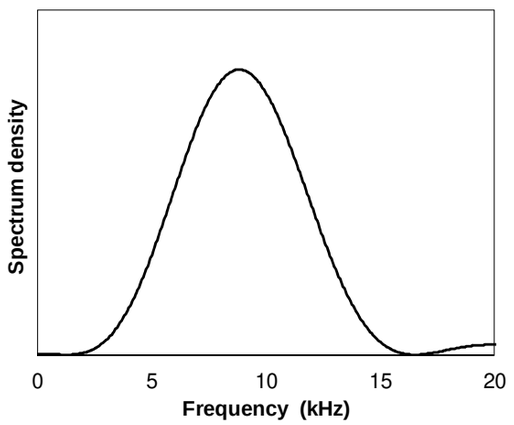

Fig. 21. Frequency spectrum of the proccessed waveform, giving characteristic peak frequncy of Rayleigh waves

5.5 Tomography reconstruction using phase velocity

All the recorded waveforms were processed for Rayleigh wave amplitudes, followed by transformation to frequency response to compute phase difference, which were used to calculate the phase velocity by utilizing Equation (1). The results were plotted against the frequency, as exemplified in Fig. 22 for the case of Rayleigh waves propagating directly from one trigger to its surrounding eight receivers. In the figure, three out of the eight dispersion curves were obtained from propagation paths that contained artificial horizontal crack in between trigger and receiver. The crack was located 30 mm from the surface. All the three paths apparently yielded reduced phase velocity values for the entire effective frequency range of excitation, which was estimated at 5-15 kHz. The phase velocity has been decreased to less than 1900 m/s in general, registering an average difference of approximately 500 m/s compared to the propagation paths containing no crack. It was interesting to note that the wavelength of Rayleigh waves as calculated based on the peak

frequency and propagation velocity was greater than the crack depth. The finding was in agreement with that of the simulation work in confirming that when the waves was effectively impinged by a horizontal crack that lied within the region of penetration, distortion was bound to occur, resulting in the change of propagation behaviour to gave lower phase velocity and translation of dispersion curve in the effective frequency range. The decrease in phase velocity due to the horizontal crack was approximately 500 m/s compared to the sound concrete and was found to be greater than that observed in the simulation work.

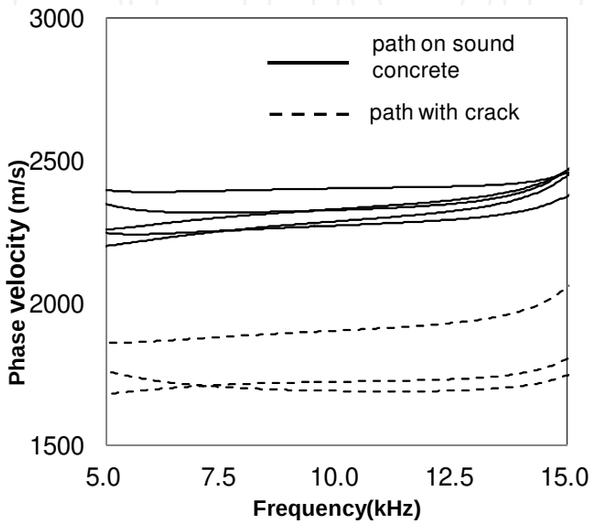

Fig. 22. Frequency spectrum of the proccessed waveform, giving characteristic peak frequncy of Rayleigh waves

For the purpose of tomography reconstruction, the measured area was divided into 6 x 6 square cells of 150 mm. The phase velocity data acquired from the peak frequency of excitation were used as the observed data and the computation process was carried out for 50 iterations to achieve satisfactory convergence. Fig. 23 presents the results of tomography reconstruction expressed in the form of phase velocity distributions for measurements from the surface with relatively small crack depths (30 mm ~ 140 mm) and large crack depths (160 mm ~ 270 mm). For measurement from the surface with small crack depths, all the four crack location were successfully detected with good visualization effect; while from the surface where the crack depths became greater, the visualization for cracks was less convincing except for the crack with 160 mm depth, which is the shallowest among the four. Based on the setting for graphical display, the cracks were indicative when the phase velocity was lower than 2000 m/s. It is also to be noted that the circular shape of the horizontal cracks was not accurately represented by the low phase velocity region and in most cases the centre of defect was indicated with the lowest value, and the change of value from the centre to the edge of defects has developed in a non-uniform way. Cracks which were not successfully visualized were due to the fact that the generated Rayleigh waves did not penetrate sufficiently deep into the concrete to be effectively impinged by these cracks. From the results it was demonstrated that the accuracy of assessment by the Rayleigh wave-based tomography was essentially dependable upon the depth of crack as well as the penetration depth.

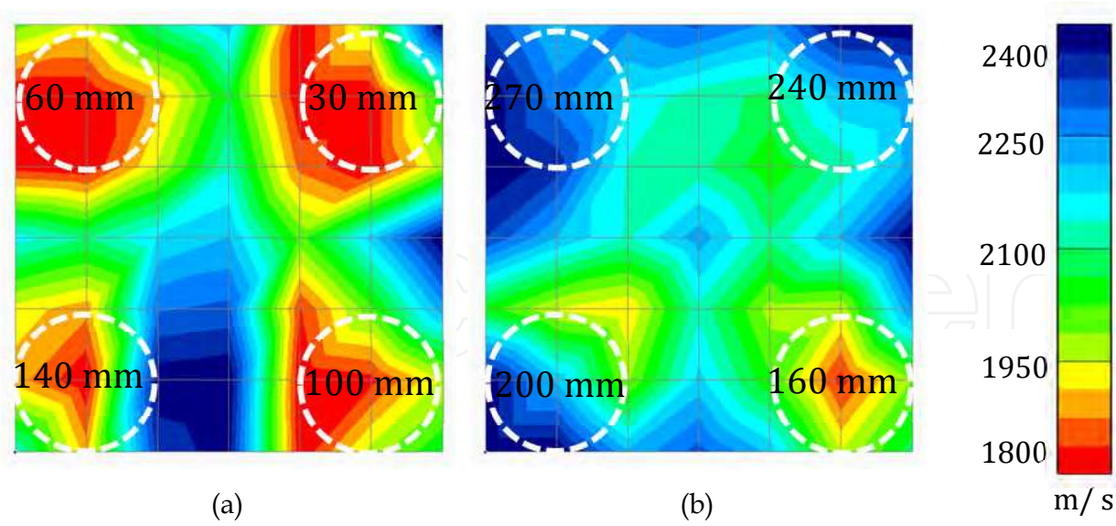

Fig. 23. Rayleigh wave tomography resutls for (a) the side with relatively small crack depth, and (b) with greater crack depth from top surface of concrete

Based on literature study, however, it is found that the penetration depth varied in accordance to material as well as structural form. For example, the was a study reporting satisfactory estimation for elastic properties of layered concrete slabs by assuming the effective Rayleigh wave penetration depth to be equivalent to half a wavelength (Wardany et. al. 1997). On the other hand, another study using concrete beams concluded that at vertical distances greater than half the beam depth, Rayleigh waves did not formed because of the fundamental modes diverged at longer wavelengths and energy was consumed in flexural mode (Zewer et. al. 2005). Also, in determining the near-surface profile of soil structures (Long & Kacaoglu 2001), it was reported that the Rayleigh wave velocity was determined primarily by the shear wave (S-wave) velocity of material in a depth range of 1/4 wavelength. Based on the findings of the current experimental study, the wavelength of Rayleigh waves has to be greater than 1.5 times the depth to crack for successful detection. The estimated wavelength, was much less than that concluded from the simulation work discussed earlier herein (2.5 times the crack depth). Nevertheless, the feasibility of utilizing the phase velocity for tomography reconstruction to detect defect in concrete has been demonstrated. It is considered further work has to be directed to refining quantitative relation between the wavelength and the depth of crack so that the vertical location of defect can be estimated in more accurately way. In any case however, it is worth mentioning that even if a crack is not visualized at its actual dimensions using the proposed method, successful detection for the fingerprint of the defect would help provide useful information for minimizing the labour and increasing the effectiveness of other pinpoint NDT techniques to characterize in detail.

6. Conclusion

The present chapter discusses elastic wave propagation of low frequency on large concrete surfaces. The objective is characterization of damage and effectiveness of repair by cement injection. A pattern of piezoelectric transducers was mounted on a large part of the surface

allowing a quick and reliable scanning of the velocity of the surface of the structure. Repair was connected to a velocity increase of the level of 5% to 6% for both longitudinal and Rayleigh waves. Furthermore, the frequency content of the pulses surviving long propagation distances increased by 15% exhibiting stronger sensitivity to the repair action. Attenuation and dispersion effects impose a dependence of measured velocity on the distance, which is more clear for longitudinal waves that travel on a shallow depth on the surface. On the other hand Rayleigh waves have a propagation depth similar to their wavelength which enables them to fly below the shallow cracks and limits their dispersion. After repair the longitudinal wave dispersion was weakened offering an additional feature sensitive to the repair effectiveness. Reliability considerations that are not normally taken into account are discussed which seem to influence the measured wave parameters.

Additionally, the feasibility of Rayleigh waves for developing a single-side access tomography technique of concrete was investigated numerically and experimentally. Tomography reconstructions results indicated the suitability of the measurement method and data analysis procedure for visualizing subsurface defects. It was demonstrated that by increasing the dominant wavelength of Rayleigh waves, wave penetration could be improved and deeper defect could be detected. Studies on the quantitative relation between dominant wavelength and depth of defect, in addition to clarifying the dispersion characteristic of Rayleigh waves are imperative in future in order to realize accurate assessment of concrete structures using the proposed tomography technique. Numerical simulations are expected to greatly enhance knowledge concerning the both the interaction between dominant wavelength and depth of defect that can be identified as well as the dependence of velocity on frequency. Nowadays, since waveform acquisition is standard to almost all ultrasonic equipment the rough characterization based on pulse velocity can be easily enhanced by features like frequency and dispersion of each wave mode. So far these have been applied successfully in laboratory conditions for material characterization but it is expected that their application in real structures will definitely improve NDT capabilities.

7. References

Aggelis, D.G., Hadjiyiangou, S., Chai, H.K., Momoki, S., Shiotani, T. (2011). Longitudinal waves for evaluation of large concrete blocks after repair, NDT&E International 44 (2011) 61–66

Aggelis D.G., Momoki S., Chai H. K. (2009). Surface wave dispersion in large concrete structures", NDT&E International 42, 304–307.

Aggelis D. G., Philippidis, T. P. (2004). Ultrasonic wave dispersion and attenuation in fresh mortar. NDT & E International, 37(8), 617-631.

Aggelis D.G., Shiotani T. (2007a). Experimental study of surface wave propagation in strongly heterogeneous media. J Acoust Soc Am; 122(5):EL151–7.

Aggelis, D.G., Shiotani, T. (2007b). Repair evaluation of concrete cracks using surface and through-transmission wave measurements, Cement & Concrete Composites 29; 700–711.

Aggelis, D. G., Shiotani, T. (2008a). Effect of inhomogeneity parameters on the wave propagation in cementitious materials. American Concrete Institute Materials Journal, 105(2), 187-193.

Aggelis, D. G., Shiotani, T. (2008b). Surface wave dispersion in cement-based media: inclusion size effect. NDT&E INT, 41, 319-325.

Aggelis, D.G., Shiotani, T., Polyzos, D. (2009). Characterization of surface crack depth and repair evaluation using Rayleigh waves. Cement and Concrete Composites, 31(1), 77-83.

Aggelis, D.G., Tsimpris, N., Chai, H.K., Shiotani, T., Kobayashi, Y. (2011). Numerical simulation of elastic waves for visualization of defects, Construction and Building Materials 25 1503–1512.

Aggelis, D. G. and T. Shiotani. (2009). An experimental study of wave propagation through grouted concrete. American Concrete Institute Materials Journal, 106(1) 19-24

Anderson, D.A., Seals, R.K. (1981). Pulse velocity as a predictor of 28- and 90-day strength, ACI J. 78– 79, 116– 122.

Chai, H.K., Aggelis, D.G., Momoki, S., Kobayashi, Y., Shiotani, T. (2010). Single-side access tomography for evaluating interior defect of concrete, Construction and Building Materials 24 2411–2418.

Chaix, J. F., Garnier V., Corneloup G. (2006). Ultrasonic wave propagation in heterogeneous solid media: Theoretical analysis and experimental validation, Ultrasonics 44, 200–210.

Diamanti, N., Giannopoulos, A., Forde, M.C. (2008) Numerical modelling and experimental verification of GPR to investigate ring separation in brick masonry arch bridges. NDT&E Int ;41:354–63.

Doyle, P.A., Scala, C.M. (1978). Crack depth measurement by ultrasonics: a review. Ultrasonics 16(4):164–70.

Graff, K.F. 1975. Wave motion in elastic solids. New York: Dover Publications.

van Hauwaert, A.; Thimus, J. F.; and Delannay, F. (1998). Use of Ultrasonics to Follow Crack Growth. *Ultrasonics*, 36 209-217.

Hevin, G., Abraham, O., Pedersen, H.A., Campillo, M. (1998). Characterisation of surface cracks with Rayleigh waves: a numerical model. NDT&E Int ;31(4): 289–97.

In, C-W., Kim, J.Y., Kurtis, K.E.,Jacobs, L.J. (2009). Characterization of ultrasonic Rayleigh surface waves in asphaltic concrete, NDT&E International 42 610–617.

Issa, C.A., Debs, P. (2007). Experimental study of epoxy repairing of cracks in concrete. Constr Build Mater;21:157–63.

Ito, F., Nakahara, F., Kawano, R., Kang, S-S., Obara, Y. (2001). Visualization of failure in a pull-out test of cable bolts using X-ray CT. Construct Build Mater 15:263–70.

Jacobs, L. J., Owino, J. O. (2000). Effect of aggregate size on attenuation of Rayleigh surface waves in cement-based materials, J. Eng. Mech.-ASCE. 126 (11) 1124-1130.

Jian, X., Dixon, S., Guo, N., Edwards, R.S., Potter, M. (2006). Pulsed Rayleigh wave scattered at a surface crack. Ultrasonics 44:1131–1134.

Jones R (1953) Testing of concrete by ultrasonic-pulse technique, Proceedings of the thirty-second annual meeting. Highway Res Board 32:258–275

Kaplan, M.F. (1959). The effects of age and water/cement ratio upon the relation between ultrasonic pulse velocity and compressive strength, Mag. Concr. Res. 11 (32) 85– 92.

Kaplan, M. F. (1960). The relation between ultrasonic pulse velocity and the compressive strength of concretes having the same workability but different mix proportions, Magazine of Concrete Research, 12 (34) 3-8.

Kase, E.J., Ross, T.A. (2003). Quality assurance of deep foundation elements, Florida Department of Transportation. In: Proceedings of the 3rd international conference on applied geophysics – geophysics 2003, Orlando, Florida, December 8–12.

Keating, J.; Hannant, D. J.; and Hibbert, A. P. (1989). Correlation between Cube Strength, Ultrasonic Pulse Velocity and Volume Change for Oil Well Cement Slurries, *Cement and Concrete Research*, 19(5); 715-726.

Kepler, W.F., Bond, L.J., Frangopol, D.M. (2000). Improved assessment of mass concrete dams using acoustic travel time tomography, part II—application. Construct Build Mater 14:147–56.

Kheder, G.F. (1999) A two stage procedure for assessment of in situ concrete strength using combined non-destructive testing. Mater Struct 32:410–417

Kinra V. K., Rousseau, C. (1987). Acoustical and optical branches of wave propagation,'' J. Wave Mater. Interaction 2, 141–152 .

Kobayashi, Y.; Shiotani, T.; Aggelis, D. G.; and Shiojiri, H. (2007). "Three- Dimensional Seismic Tomography for Existing Concrete Structures,"*Proceedings of the Second International Operational Modal AnalysisConference*, IOMAC 2007, (April 30-May 2, Copenhagen), V. 2.pp. 595-600.

Long, L. T., Kacaoglu, A. (2001). Surface-wave group-velocity tomography for shallow structures. J Env Eng Geophys 6(2); 71-81.

Landis, E. N., Shah, S. P. (1995). Frequency-dependent stress wave attenuation in cement-based materials, J. Eng. Mech.-ASCE 121 (6) 737-743.

Liu, P.L., Lee, K.H., Wu, T.T., Kuo, M.K. (2001). Scan of surface-opening cracks in reinforced concrete using transient elastic waves. NDT&E Int 34:219–26.

Mikulic, D., Pause, Z., Ukraincik, V. (1999). Determination of concrete quality in a structure by combination of destructive and non-destructive methods. Mater Struct 25:65–69

Monteiro, P. J. M., Helene, P. R. L., Kang, S. H. (1993). Designing concrete mixtures for strength, elastic modulus and fracture energy, Materials and Structures, 26 443-452

Naik TR, Malhotra VM, Popovics JS. (2004).The ultrasonic pulse velocity method. In: Malhotra VM, Carino NJ, editors. Handbook on nondestructive testing of concrete. Boca Raton: CRC Press.

Ohtsu M, Tomoda Y. (2008). Phenomenological model of corrosion process in reinforced concrete identified by acoustic emission. ACI Mater J. 105(2):194–9.

Ohtsu, M., Alver, N. (2009). Development of non-contact SIBIE procedure for identifying ungrouted tendon duct. NDT&E Int 42:120–7.

Ono, K. (1988) Damaged Concrete Structures in Japan due to Alkali Silica Reaction," *The International Journal of Cement Composites and Lightweight Concrete*, 10;4 247-257.

Owino, J. O., Jacobs, L. J. (1999). Attenuation measurements in cement-based materials using laser ultrasonics, J. Eng. Mech.-ASCE. 125 (6) 637-647.

Pecorari, C. (2001). Scattering of a Rayleigh wave by a surface-breaking crack with faces in partial contact. Wave Motion ;33:259–70.

Philippidis, T. P., Aggelis D. G. (2003) An acousto-ultrasonic approach for the determination of water-to-cement ratio in concrete. Cement and Concrete Research, 33(4), 525-538.

Philippidis, T. P., Aggelis, D. G. (2005). Experimental study of wave dispersion and attenuation in concrete. Ultrasonics, 43(7), 584-595.

Popovics, S. (2001). Analysis of the Concrete Strength versus Ultrasonic Pulse Velocity Relationship," *Materials Evaluation*, 59(2) 123-130.

Punurai W, Jarzynski J, Qu J, Kurtis KE, Jacobs LJ. (2006). Characterization of entrained air voids in cement paste with scattered ultrasound. NDT&E Int 2006;39(6):514–24.

Qasrawi HY (2000) Concrete strength by combined nondestructive methods simply and reliably predicted. Cem Concr Res 30:739–746

Qixian L., Bungey J.H. (1996). Using compression wave ultrasonic transducers to measure the velocity of surface waves and hence determine dynamic modulusof elasticity for concrete. Construct Build Mater 4(10):237–42.

Sachse, W., Pao, Y.-H. (1978). On the determination of phase and group velocities of dispersive waves in solids, J. Appl. Phys. 49 (8) 4320–4327.

Sansalone, M.J., Streett, W.B. (1997). Impact-echo nondestructive evaluation of concrete and masonry. Ithaca, NY: Bullbrier Press.

Sayers C. M., Dahlin, A. (1993). Propagation of ultrasound through hydrating cement pastes at early times, Advanced cement based materials, 1:12-21.

Sassa K. (1988). Suggested methods for seismic testing within and between boreholes. Int J Rock Mech Min Sci Geomech Abstr;25(6):449–72.

Shah, S.P., Popovics, J.S., Subramanian, K.V., Aldea, C.M. (2000). New directions in concrete health monitoring technology, J. Eng. Mech.—ASCE 126 (7) 754–760.

Shiotani, T., Aggelis D. G. (2009). Wave propagation in concrete containing artificial distributed damage. Materials and Structures, 42(3), 377-384.

Shiotani, T., Momoki, S., Chai, H. K., Aggelis, D.G. (2009). Elastic wave validation of large concrete structures repaired by means of cement grouting, Construction and Building Materials 23 2647–2652.

Shiotani, T., Aggelis, D. G. (2007). Evaluation of repair effect for deteriorated concrete piers of intake dam using AE activity. Journal of Acoustic Emission, 25, 69-79.

Song, W.J., Popovics, J.S., Aldrin, J.C., Shah, S.P. (2003). Measurements of surface wave transmission coefficient across surface-breaking cracks and notches in concrete. J Acoust Soc Am 113(2):717–25.

Thanoon, W.A., Jaafar, M.S., Razali, M., Kadir, A., Noorzaei, J. (2005). Repair and structural performance of initially cracked reinforced concreteslabs. Constr Build Mater 19(8):595–603.

Tsinopoulos, S. V., Verbis, J. T., Polyzos, D. (2000). An iterative effective medium approximation for wave dispersion and attenuation predictions in particulate composites,'' Adv. Composite Lett. 9, 193–200.

Tsutsumi, T., Wu, J., Wu, J., Huang, X., Wu, Z. (2005). Introduction to a new surface-wave based NDT method for crack detection and its application in large dammonitoring. In: Proceedings of international symposium on dam safety and detection of hidden troubles of dams and dikes, 1–3 November, Xian, China (CD-ROM).

Yokota, O., Takeuchi, A. (2004). Injection of repairing materials to cracks using ultrasonic rectangular diffraction method. In: 16th World conference on non destructive testing 2004 (WCNDT), Montreal, Canada, August 30–September 3.

Zerwer, A., Polak, M.A., Santamarina, J.C. (2005). Detection of surface breaking cracks in concrete members using Rayleigh waves. J Environ Eng Geophys;10(3): 295–306.

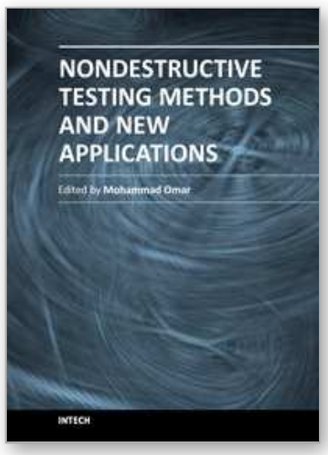

Nondestructive Testing Methods and New Applications

Edited by Dr. Mohammad Omar

ISBN 978-953-51-0108-6
Hard cover, 264 pages
Publisher InTech
Published online 02, March, 2012
Published in print edition March, 2012

Nondestructive testing enables scientists and engineers to evaluate the integrity of their structures and the properties of their materials or components non-intrusively, and in some instances in real-time fashion. Applying the Nondestructive techniques and modalities offers valuable savings and guarantees the quality of engineered systems and products. This technology can be employed through different modalities that include contact methods such as ultrasonic, eddy current, magnetic particles, and liquid penetrant, in addition to contact-less methods such as in thermography, radiography, and shearography. This book seeks to introduce some of the Nondestructive testing methods from its theoretical fundamentals to its specific applications. Additionally, the text contains several novel implementations of such techniques in different fields, including the assessment of civil structures (concrete) to its application in medicine.

How to reference

In order to correctly reference this scholarly work, feel free to copy and paste the following:

D. G. Aggelis, H. K. Chai and T. Shiotani (2012). Elastic Waves on Large Concrete Surfaces for Assessment of Deterioration and Repair Efficiency, Nondestructive Testing Methods and New Applications, Dr. Mohammad Omar (Ed.), ISBN: 978-953-51-0108-6, InTech, Available from: http://www.intechopen.com/books/nondestructive-testing-methods-and-new-applications/elastic-waves-on-large-concrete-surfaces-for-assessment-of-deterioration-and-repair-efficiency

INTECH
open science | open minds

InTech Europe
University Campus STeP Ri
Slavka Krautzeka 83/A
51000 Rijeka, Croatia
Phone: +385 (51) 770 447
Fax: +385 (51) 686 166
www.intechopen.com

InTech China
Unit 405, Office Block, Hotel Equatorial Shanghai
No.65, Yan An Road (West), Shanghai, 200040, China
中国上海市延安西路65号上海国际贵都大饭店办公楼405单元
Phone: +86-21-62489820
Fax: +86-21-62489821

IntechOpen